Binding and release of cholesterol in the Osh4 protein of yeast

ARTICLE *in* PROTEINS STRUCTURE FUNCTION AND BIOINFORMATICS · MAY 2009

Impact Factor: 2.63 · DOI: 10.1002/prot.22263 · Source: PubMed

3 AUTHORS, INCLUDING:

Jeffery Klauda
University of Maryland, College Park
93 PUBLICATIONS **2,437** CITATIONS

Published in final edited form as:
Proteins. 2009 May 1; 75(2): 468–477. doi:10.1002/prot.22263.

Binding and Release of Cholesterol in the Osh4 Protein of Yeast

Rishi P. Singh[1], **Bernard R. Brooks**[1], and **Jeffery B. Klauda**[1,2,*]

[1]Laboratory of Computational Biology, National Heart, Lung, and Blood Institute, National Institutes of Health, Bethesda, MD 20892-9314

[2]Department of Chemical and Biomolecular Engineering, University of Maryland, College Park, MD 20742

Abstract

Sterols have been shown experimentally to bind to the *Osh*4 protein (a homolog of the oxysterol binding proteins) of *Saccharomyces cerevisiae* within a binding tunnel, which consists of antiparallel β-sheets that resemble a β-barrel and three α-helices of the N-terminus. This and other *Osh* proteins are essential for intracellular transport of sterols and ultimately cell life. Molecular dynamics (MD) simulations are used to study the binding of cholesterol to *Osh*4 at the atomic level. The structure of the protein is stable during the course of all MD simulations and has little deviation from the experimental crystal structure. The conformational stability of cholesterol within the binding tunnel is aided in part by direct or water-mediated interactions between the 3-hydroxyl (3-OH) group of cholesterol and Trp^{46}, Gln^{96}, Tyr^{97}, Asn^{165}, and/or Gln^{181} as well as dispersive interactions with Phe^{42}, Leu^{24}, Leu^{39}, Ile^{167}, and Ile^{203}. These residues along with other nonpolar residues in the binding tunnel and lid contribute nearly 75% to the total binding energy. The strongest and most populated interaction is between Gln^{96} and 3-OH with a cholesterol/Gln^{96} interaction energy of □4.5±1.0 kcal/mol. Phe^{42} has a similar level of attraction to cholesterol with □4.1±0.3 kcal/mol. A MD simulation without the N-terminus lid that covers the binding tunnel resulted in similar binding conformations and binding energies compared to simulations with the full-length protein. Steered MD was used to determine details of the mechanism used by *Osh*4 to release cholesterol to the cytoplasm. Phe^{42}, Gln^{96}, Asn^{165}, Gln^{181}, Pro^{211}, and Ile^{206} are found to direct the cholesterol as it exits the binding tunnel, as well as Lys^{109}. The mechanism of sterol release is conceptualized as a *molecular ladder* with the rungs being amino acids or water-mediated amino acids that interact with 3-OH.

Keywords

Molecular simulation; molecular dynamics; oxysterol binding proteins; sterol transport; protein function; steered molecular dynamics

Introduction

The intracellular transport of sterols between organelles in cells can involve vesicular or nonvesicular transport mechanisms. Vesicles that bud from donor membranes move along microtubules or actin filaments to the acceptor membrane.1 This transport requires metabolic energy to move the vesicle along an intact cytoskeleton. Nonvesicular transport of sterols involves proteins that bind to sterols and selectively transport them to other cellular membranes.1 The oxysterol binding proteins (OSBPs) and its homologues (OSHs) are believed to mediate the trafficking of sterols,2،3 as well as other proteins, e.g., Steroidogenic

*To whom correspondence should be addressed: jbklauda@umd.edu, Phone: (301) 405-1320, Fax: (301) 314-9126

acute regulatory protein (StAR).4 The OSH/OSBP proteins are essential for eukaryotic and mammalian cell life in maintaining the intracellular distribution of sterols.2،5،6 OSBPs and OSHs are known to shuttle sterols to/from organelles in the cell, such as, from the endoplasmic reticulum to the plasma membrane.7

For yeast, seven OSHs genes together control the local sterol concentration. The deletion of all the *Osh* proteins results in cell death. Although cells do not die with the deletion of one *Osh* gene, the structure of the membrane can be severely altered.5 The OSH family of proteins also exists in mammals with several additional proteins beyond yeast.8 ORP4 (mammalian analog of *Osh*4 in yeast) is distributed in the brain, heart, and muscle tissues. Cells that over-express this protein have a 40% reduction in LDL-derived cholesterol.8 ORP4 is also expressed in human cancer cell lines and solid tumors, which suggests that ORP4 could be used as a tumor marker.2 However, it is unclear if ORPs are directly involved in the development of malignant cells.

Recently, Im et al.6 determined the structure of *Osh*4 in yeast (*Saccharomyces cerevisiae*) complexed with ergosterol, cholesterol, and three hydroxycholesterols. All the sterols are located inside the hydrophobic tunnel of *Osh*4 (Fig. 1) and cholesterol preferentially binds to this protein. *Osh*4 consists of central antiparallel β-sheets that resemble a β-barrel and three α-helices of the N-terminus which together forms the binding tunnel for sterols (Fig. 1). The first 29 residues form a lid that covers the tunnel opening and has been suggested to aid in preventing sterol release to the cytoplasm. *Osh*4-*apo* or the open state preferentially binds to the phosphates of the lipid head group via Lys residues to allow for sterol uptake. The transport of sterols between membranes is enhanced with membranes that contain phosphoinositides.6 However, little is known about the atomic-level mechanism for sterol uptake from the endoplasmic reticulum and its release to the cytosol or plasma membrane.

Computational techniques, such as molecular dynamics (MD), are useful in determining atomic-level details of substrate binding9-12 and transport mechanisms in proteins10،12،13. Previously, docking, MD, and steered-MD have been used to study cholesterol binding and its release mechanism from the StAR proteins.12 A more recent study by Canagarajh et al. 14 has used molecular simulations to investigate *Osh*4 structural changes in response to cholesterol binding and release. In our paper, MD simulations of *Osh*4 in solution will be used to describe cholesterol binding and compare it with the known experimental crystal structure. The structure, dynamics, and energetics of binding will be the focus of these simulations. The sterol binding of *Osh*4 without the lid residues will test the stability of cholesterol binding in the absence of the binding tunnel cover. Important protein/cholesterol interactions (dispersive and electrostatic) will be determined during a simulation of sterol release to the cytoplasm. We will conclude with a proposed model for sterol release to the cytoplasm by *Osh*4, i.e., atomic-level machinery described here as a *molecular ladder*.

Methods

The full-length *Osh*4 protein and that without the lid (*Osh*4-noLid, first 31 residues deleted) are simulated with the CHARMM15 and NAMD16 programs. NAMD, by the end of the experimentation, adopted the CHARMM C22/CMAP force field and scaled better, allowing for more time efficient runs. The lid, binding tunnel and other important parts of *Osh*4 are labeled in Fig. 1. Residue numbering in this paper follows that of Im et al.6 The crystal structure contains two additional residues to the N-terminus (Met^{-1} and Asp^{0}) and these are also used in our simulations, so even though Pro^{1} is the third residue in these simulations it will be referred as residue 1. Standard CHARMM patches for the C- and N-terminus were used for this protein. The CHARMM family of force fields are used to describe the atomic

interactions of the protein17¯20 and cholesterol21; TIP3P consistent with CHARMM parameters22،23 is used to model water.

For the CHARMM and NAMD simulations, Lennard-Jones (LJ) interactions are smoothed by a switching function over 10 to 12 Å.15 Particle mesh Ewald (PME)24 is used for the long-range (beyond 12 Å) electrostatic contribution to the total energy. Extended system formalism is used to maintain the pressure with a barostat at 1 bar.25،26 For the CHARMM runs, the temperature (310.15 K) is held constant with the Hoover thermostat27 and a thermostat coupling constant of 20,000 kcal mol^{-1} ps^{-2}. Since NAMD does not have temperature control beyond Langevin dynamics, the temperature was rescaled every 1ps for the first 0.5ns in equilibration and then unscaled for the remainder of the simulation (*NPH* ensemble). All hydrogen atoms are constrained using the SHAKE algorithm.28 A time step of 1 fs was used for all simulations except steered MD (SMD)29،30 with 2 fs.

For all simulations, the initial protein conformation was the x-ray crystal structure (1ZHY, Fig. 1).6 The crystallographic waters in the 1ZHY structure are included as well as the placement of cholesterol (Chol). This protein has a net charge of □10, so ten sodium ions are included to maintain electroneutrality. Additional waters are used to solvate *Osh*4 in rhombic dodecohedran (RHDO) unit cell for the MD simulation of the full-length protein. RHDO is pseudo-spherical in shape so the amount of water required is less than a cubic box. Since NAMD cannot simulate complex crystal repeating units, simulations of *Osh*4-noLid and *Osh*4/SMD use a cubic repeating cell. Previously equilibrated TIP3P water is added in all cases such that unphysical interactions do not exist between the protein and its image. The MD simulation with the RHDO unit cell has 49,642 atoms and the SMD simulation is the largest system with 93,502 atoms.

With these starting conformations, the energy was minimized with the steepest decent routine for 300 steps to reduce unfavorable van der Waals contacts. The system was then equilibrated for 0.5 ns at 310.15 K before running the production runs that are discussed here. The full-length *Osh*4 protein is simulated with unbiased MD for 25 ns to determine the stability of cholesterol binding to the protein (CHARMM). A 14-ns NAMD simulation of *Osh*4-noLid is used to determine the influence of the lid on cholesterol binding. To enhance the release of cholesterol from the binding tunnel, two constant velocity (cv) SMD29،30 simulations are used to pull the sterol (each with different initial velocities). Cholesterol is pulled along a vector defined by the bottom of the binding tunnel and lid opening with a force constant of 300.15 pN Å and a velocity of 1×10^{-3} Å/ps. This pulling velocity is half the speed of the slowest SMD simulation by Canagarajah et al.14 to allow for minimal disturbance in the exit pathway. The force constant is also identical to a similar simulation with the protein lactose permease.13 Harmonic restraints (k_h = 200 kcal/mol/$Å^2$) on the protein backbone are used to prevent the pulling of the entire protein for residues at the side opposite of the lid (49-62, 77-88, 155-158, 188-193, and 224-227) and thus fixing the position of *Osh*4. These restraints are a sufficient distance from the binding tunnel to not influence specific protein/cholesterol interactions.

All analysis of these simulations, in part, involves the use of CHARMM routines. The binding energy of each conformation (sampled every 1ps) is estimated from these trajectories by

$$\Delta E_j^{\text{bind}} = E_j^{\text{system}} - E_j^{\text{chol}} - E_j^{\text{Prot/sol'n}} \quad (1)$$

The average binding energy, $\langle \Delta E^{\text{bind}} \rangle$, is reported relative to the solvation energy,

$$\left\langle \Delta\Delta E^{\text{bind/sol}} \right\rangle = \left\langle \Delta E^{\text{bind}} \right\rangle - \left\langle \Delta E^{\text{sol}} \right\rangle \quad (2)$$

where a negative $\langle \Delta\Delta E^{\text{bind/sol}} \rangle$ represent a preference to protein binding over the solution phase ignoring entropic effects. A 20-ns simulation of cholesterol in water was used to determine ΔE^{sol}, which is □45.35±0.04 kcal/mol.

Hydrogen bonds are classified between a donor and acceptor if the distance is less than 3.2 Å. The root-mean squared deviation (RMSD) from the 1ZHY crystal structure and fluctuations (RMSF) are determined for the backbone of *Osh*4. The visual molecular dynamics (VMD) program was used to make all molecular figures.31

Results

MD of Osh4/Chol

The structure of the protein did not change dramatically during the course of the 25-ns MD simulation (Fig. 2, top left). The ⟨RMSD⟩=1.66±0.16 Å for the backbone of the entire protein. The lid of *Osh*4 covers the binding tunnel throughout the simulation, but has a larger ⟨RMSD⟩ of 1.92±0.20 Å. The first few residues of the N-terminus are the most flexible and change orientation with respect to the α_1 helix (Fig. 1). The lid is stabilized by hydrogen bonds and hydrophobic interactions (Fig. 3a). The first five N-terminus residues are stabilized by a hydrophobic interaction between the side-chain rings of Tyr^4 and Phe^{32} and occasionally with water-mediated Tyr^4/backbone-Phe^{32} hydrogen bonds. Since water-mediated interactions are weaker than direct hydrogen bonds, these residues tend to have more flexibility compared to the α_1 helix. The configuration of the lid covering the binding tunnel is also stabilized by intra-loop and α_1-loop hydrogen bonds (Fig. 3a). A direct Asp^{23}/Ser^{26} hydrogen bond and water-mediated Ser^{16}/Ser^{28} hydrogen bonds contribute to the stability of this lid-covering conformation. In this simulation, helix α_7 has limited displacement from the crystal structure.

The binding conformations are extremely stable with only minor changes in *Osh*4/Chol interactions (Fig. 3b-d). The crystal structure contains6 a direct hydrogen bond between Gln^{96} and the 3-hydroxyl group (3-OH) of cholesterol. In addition, water-mediated interactions are observed between 3-OH and Trp^{46}, Tyr^{97}, Asn^{165}, and Gln^{181}. For our MD simulations, water-mediated protein/cholesterol interactions are common to all binding configurations. Initially, during the first half of the simulation (excluding the first ns), water mediates the interaction between Gln^{96} and 3-OH, but during the second half of the simulation, a direct hydrogen bond can exist. However, water-mediated Gln^{96}/3-OH interactions dominate with only 16.6% of the simulation containing a direct hydrogen bond. As seen in the crystal structure, water-mediated interactions also exists between and Trp^{46}, Tyr^{97}, Asn^{165}, and Gln^{181}. However, interactions with the residues on the β_6 or β_7 sheets are less common. The least common cholesterol/protein interaction is with Tyr^{97}; it rarely has one water to mediate its interaction with 3-OH and typically involves two waters.

Water in the hydrated polar cluster at the bottom of the tunnel can be positionally stable in that it does not escape from the region during the 25-ns simulation. For example, the same water molecule exists in all three snapshots in Fig. 3b-d and exchanges its hydrogen bond donor/acceptor modes with Phe^{42}, Tyr^{46}, Gln^{96}, and 3-OH. This water, part of the original solvation structure (not the crystal), is typically coordinated with Phe^{42}, Gln^{96}, and 3-OH and occasionally with Tyr^{46}. The probability of having at least one hydrogen bond between these three residues and the 3-OH of cholesterol is 0.99. The probability of having at least three hydrogen bonds is 0.45. Since these probabilities are based on a water molecule that is

trapped in the binding site, they may not be equilibrium probabilities and subject to the initial conditions (or conditional probabilities).

Table 1 contains the average of significant protein-cholesterol interaction energies for the entire simulation. Cholesterol has the strongest interaction energy with the polar residues of Gln^{96}, Tyr^{97}, and Lys^{109}. Gln^{96} has the highest attraction to cholesterol and is consistent with the direct and water-mediated interactions. Phe^{42} has the strongest interaction with cholesterol for all the non-polar residues of *Osh*4, but other residues are moderately attracted to cholesterol (Leu^{24}, Leu^{39}, Ile^{167}, and Ile^{203}). The hydrophobic residues of the lid Trp^{10}, Phe^{13}, Leu^{14}, Ile^{17}, and Phe^{20} (not listed in Table 1) all have weak to no interaction with cholesterol.

The affinity of *Osh*4 for cholesterol is known to be high6 and the total binding energy for the *Osh*4/Chol simulation reflects this result. The $\Delta\Delta E^{bind/sol}$ = □14.13±0.23 kcal/mol, which implies that the bound state is more favored compared to cholesterol in solution (ignoring entropic effects). The total van der Waals (vdW) contribution to the binding energy of cholesterol is 82%, which suggests that vdW dominates over electrostatics. Residues in Table 1 and other nonpolar residues in the binding tunnel and lid account for ~75% of the total binding energy, which suggests local interactions within the binding cavity contribute significantly to the total binding energy. These local interactions partially aid in the conformational stability of cholesterol within the binding tunnel.

MD of Osh4-noLid/Chol

Similar to the previously described simulation, the structure of the protein without the lid did not change significantly from the x-ray crystal structure.6 The ⟨RMSD⟩ from the crystal structure was 1.71±0.16 Å for the backbone of the protein (Fig. 2, top right) and is similar to that of the *Osh*4 25-ns simulation. The lid has no major influence on the overall structure of the remaining protein at least on these short timescales.

The sterol binding conformations of the *Osh*4-noLid/Chol simulation are very similar to the full-length *Osh*4. The 3-OH group of the cholesterol typically forms direct hydrogen bonds or water-mediated interactions with Gln^{96}, Gln^{181}, and Phe^{42} with binding conformations similar to those shown in Fig. 3. Comparable to the full-length *Osh*4 simulation, cholesterol did not deviate from its position within the polar pocket of the protein. Water molecules in the bottom of the binding tunnel remain stable, while the flexible glutamines reach for the 3-OH group of cholesterol. Moreover, the interaction energies between the protein and cholesterol are similar except the lack of interactions with the lid residues (Table 1).

The binding energy for the simulations of *Osh*4 with and without the lid are statistically equivalent ($\Delta\Delta E^{bind/sol}$ = □14.09±0.11 kcal/mol). For binding energetics, the lid essentially has no effect on the binding energy and the bottom of the binding tunnel contributes the most to the stability of this bound state.

SMD of Osh4/Chol

Since cholesterol did not exit the binding site for the other two simulations, two cv-SMD were used to guide cholesterol towards the lid and then begin to exit the binding tunnel. Although cv-SMD adds an unphysical pulling force, important *Osh*4/Chol interactions can be determined as the sterol exits the binding site. Since it is believed there exists only one exit pathway,6،14 testing of multiple directions for sterol exit from the binding pocket is not required. The block-averaged pulling force and distance time series are shown in Fig. 4 for both trajectories. Typically raw forces above 150-250 pN represent important protein/cholesterol interactions that require a higher pulling force to maintain a constant velocity.

Block-averaged forces above this amount relate to general protein/cholesterol interactions that cease after this peak.

Initially, cholesterol has similar binding conformations to that of the two MD simulations. The hydroxyl group on cholesterol interacts with one or more amino acids (Tyr^{46}, Gln^{96}, Asn^{165}, and Gln^{181}) either water-mediated or direct hydrogen bonds. However, the primary interactions are with Gln^{96} and Gln^{181}. The first transitional evident is the increase in average force between 2 and 4 ns for both SMD simulations, which corresponds to average interaction energies between cholesterol and these two residues of □4 to □8 kcal/mol (each), which are primarily electrostatic in nature. This is the final breaking of direct or water-mediated Asn^{165} and/or Gln^{181}/cholesterol hydrogen bonds. In general, with the increased distance from the binding site after this first transition, water-mediated hydrogen bonds replace the direct hydrogen bonds. The vdW contacts that have the largest interaction with cholesterol are Phe^{42} (□4 kcal/mol) and Ile^{167} (□2.5 kcal/mol) and the interactions dissipate after this time period, especially Phe^{42}.

Gln^{96} and Gln^{181} are fairly flexible and interact with cholesterol throughout the first half of the simulation, but Gln^{96}/cholesterol interaction is more common. . After the initial transition (~4 ns), these protein/cholesterol hydrogen bonds are always water-mediated (Fig. 5a). Gln^{96} acts both as a hydrogen acceptor and donor via the amine and carboxyl groups and Gln^{181} primarily as an acceptor. The highest peak at ~7 ns for run 1 (SMD1) represents the final hydrogen bond with the residues in the bottom of the tunnel (Gln^{96}). After this, Gln^{96} retracts to the tunnel end and has a direct hydrogen bond with Phe^{42} (Fig. 5b) that exists in the *Osh*4-*apo* crystal structure.6 Gln^{96} appears to act as a guide to direct cholesterol to/from the binding tunnel. The second SMD run (SMD2) did not result in such a strong force peak at ~7 ns but similar water-mediated interactions exists between 4.5-6.5 ns with Gln^{96}/Gln^{181} and cholesterol.

The third transition exists at around 10-12 ns, where Lys^{109} has a weak interaction with cholesterol via water-mediation (Fig. 5c). This is the final transition that involves direct or indirect interactions between *Osh*4 and cholesterol. Moreover, during this time period vdW interactions with cholesterol and Ile^{206}, Pro^{211}, and Phe^{171} have marked increases in their interactions energies of approximately □4 to □5, □2.5, and □1.5 kcal/mol, respectively.

During the last few nanoseconds of the SMD simulation, the hydrophobic half of the lid interacts with the hydrophobic tail of cholesterol and holds the cholesterol within the cavity. In general, the lid covers the binding tunnel and is stabilized primarily by hydrophobic interactions with the remainder of the protein. However, the hydrogen bond pair within the loop that bends the lid over the binding tunnel opening (residues 20-28) maintains this turn (Asp^{23}/Ser^{26}). The final increase in the average force at 14-15 ns (SMD1) is the result of cholesterol pushing against the lid and surrounding residues (Fig. 5d). The lid in the SMD2 simulation is displaced from the opening and the average forces are reduced compared to the SMD1 run. No hydrogen bonding between cholesterol and *Osh*4 exists during this final transition, but compared to the initial position of cholesterol there is an increase in certain vdW interactions between cholesterol and the protein. The highly conserved residues (in all OSH/ORP proteins in humans and yeast) of Leu^{24}, Leu^{27}, Ile^{206} have interaction energies of □1.0, □2.5, and □4.0 kcal/mol, respectively. Moreover, Ala^{29}, Ile^{33}, and Pro^{211} all have increased interactions with cholesterol (□2, □3, and □1.5 kcal/mol, respectively). Transient interactions with the lid residues of Trp^{10}, Phe^{13}, Leu^{14}, Ile^{17}, and Phe^{20} depend on the pulling simulation, but for at least one simulation have interaction energies of at least □3 kcal/mol per residue.

The RMSD from the x-ray crystal structure6 is shown as a time series in Fig. 2 (bottom) for the two SMD trajectories. The first halves of the trajectories are similar in deviation as the *Osh*4/Chol MD simulation. However, for the SMD1 trajectory at 5 ns helix α_7 displaces significantly from the crystal structure. Additional, structural changes happen during the second half (7.5-15 ns) of the SMD *Osh*4/Chol simulations. The first significant increase in RMSD of the SMD1 trajectory (~8 ns) is the result of movement of the first ten N-terminus residues and an orientation nearly colinear with the α_1 helix of the lid. This orientation returns to being nearly perpendicular to the α_1 helix for most of the remaining simulation. The large increase in the RMSD in the final three nanoseconds of both trajectories is the result of cholesterol distorting the overall lid structure (SMD1) or displacement of the lid (SMD2).

Discussion and Conclusion

The protein structure of the full-length *Osh*4 simulations remains stable during the entire simulation. The 25-ns MD simulation results in a low ⟨RMSD⟩ (1.66±0.16 Å) of the protein backbone compared to the x-ray crystal structure. The protein lid is one of the more mobile parts of *Osh*4 with RMSF of the backbone of greater than 1 $Å^2$ and agrees with the high experimental B-factors.6 Many residues in the lid contain B-factors in the range of 30-45 $Å^2$ which is higher than the average B-factor of 25 $Å^2$ for all protein residues. For the *Osh*4 MD simulation, this mobility primarily involves the displacement of the first five N-terminal residues and movement of the last 10 residues. It is not until cholesterol is forced out of the binding tunnel does the overall lid structure change (Fig. 5d). During the last nanosecond of the cv-SMD trajectories, only the direct Asp^{23}/Ser^{26} hydrogen bond remains to hold the lid over the binding tunnel. This polar/polar pair is conserved for all seven yeast proteins and twelve human equivalent ORPs.6 The polar-acidic/polar-neutral paring of Asp^{23}/Ser^{26} in *Osh*4 is less common than a polar-acidic/polar-basic paring, but the latter forms stronger salt bridge interactions. It is likely that these two residues are important for the stability of the lid orientation over the binding tunnel for all OSH/ORP proteins.

The x-ray structures of the *apo* and bound form of *Osh*4 differ primarily in the orientation of helix α_7.6 Recent simulations suggest that the movement of α_7 is conformationally coupled with the opening of the lid and thus creates a docking site for the membrane.14 In our work, only a single trajectory for the cv-SMD simulation (SMD1) results in a significant structural change of α_7 (Fig. 2). The MD simulations with cholesterol bound to *Osh*4 did not result in a significant change in α_7, but the RMSF can vary from 1 to 1.8 $Å^2$ for these residues. Although the movement of α_7 may be coupled with the lid based on *Osh*4-*apo* simulations, 14 this was not observed for our simulations. Additional simulations for the *Osh*4 without a bound sterol may likely be required to detect such coupling.

The crystal structure of *Osh*4/Chol has a binding structure with one direct hydrogen bond between Gln^{96} and the 3-hydroxyl (3-OH) group of cholesterol. Although our MD simulations have direct Gln^{96}/3-OH hydrogen bonds, water-mediated interactions are more common between this residue and cholesterol (Fig. 3). Water-mediated interactions also exists between 3-OH and Trp^{46}, Tyr^{97}, Asn^{165}, and $Gln,^{181}$ which are in excellent agreement with the x-ray structure. The stability of water/cholesterol or water/protein interaction can be extremely high such that water does not displace from the 3-OH binding site during the entire 25-ns simulation. In the *Osh*4/Chol simulation, the same water molecule acts as a hydrogen bond donor/acceptor with at least Phe^{42}, Tyr^{46}, Gln^{96}, or 3-OH; Tyr^{46} interacts only slightly with this water (hydrogen bonds form only 8.1% during the 25-ns simulation). Since cholesterol lacks consistent direct protein hydrogen bonds, water-mediated interactions are important for the stability of sterol binding. The four polar residues important in cholesterol binding to the bottom of the tunnel (Gln^{96}, Tyr^{97}, Asn^{165},

and Gln^{181}) are not conserved across yeast OSHs and human ORPs. Important residues in the binding tunnel may be particular to each protein because of its specificity for different sterols and lipids.

The binding energy of cholesterol to *Osh*4 is dominated by the vdW interactions. The relative binding energy to that of cholesterol solution ($\Delta\Delta E^{bind/sol}$) for full-length *Osh*4 and *Osh*4-noLid is □14.13±0.23 and □14.09±0.11 kcal/mol, respectively. The lack of a lid has essentially no effect on the binding energy of cholesterol. The vdW contribution to the binding energy of cholesterol is roughly 80%, which is to be expected because of cholesterol's ring structures and its vdW interactions with similar amino acids via π stacking. Although sterols have been suggested to stabilize the lid through direct vdW interactions,6 this has a minimal effect on the binding of cholesterol based on a comparison of the *Osh*4 and *Osh*4-noLid simulations. Moreover, Leu^{24} is the only lid amino acid that has a moderately strong interaction with cholesterol (Table 1). Trp^{10}, Phe^{13}, Leu^{14}, Ile^{17}, and Phe^{20} have only weak interactions with cholesterol, which differs from similar simulations of Canagarajah et al.14 where they suggest that these residues are tightly bound to the tail of cholesterol. Only Phe^{13} has weak to moderate binding (□0.83 kcal/mol). Therefore, this does not suggest that these residues are "tightly" bound to cholesterol. The electrostatic contribution to the binding energy is dominated by interactions with sterol and the residues at the bottom of the binding tunnel. The dominant electrostatic interaction is with Gln^{96} which occasionally forms a direct hydrogen bond with the 3-OH group of cholesterol resulting in an interaction energy of approximately □7 kcal/mol.

Cholesterol remains within the binding tunnel for both the *Osh*4 and *Osh*4-noLid simulations. Water freely exchanging with the solution phase has no effect on cholesterol binding. It is likely that the polar interactions between the *Osh*4 lid and phospholipids in a membrane opens up the protein and enhances the ability of cholesterol to leave the binding tunnel, i.e., the hydrophobic tail of cholesterol prefers the center of the membrane compared to water.

Since cholesterol did not move from the bottom of the binding tunnel, cv-SMD simulations were used to determine important protein/cholesterol interactions that exist as the sterol leaves the binding tunnel. Initially, as the cholesterol is pulled from the binding site, the sterol conformations are similar to that of the two MD runs. Direct or water-mediated interactions with Asn^{165} end at a 2.4 Å cholesterol distance (Fig. 4) from its initial position (3.5 ns). Water-mediated interactions with 3-OH and Gln^{96} or Gln^{181} exist after 3.5 ns and terminate at about 7 ns (5.6 Å). Phe^{42}, Ile^{167}, Ile^{203}, and Leu^{201} have vdW interactions with cholesterol when the sterol is in the binding pocket. Lys^{109} interacts weakly via water-mediation with 3-OH around 10-12 ns as well as other vdW interactions (Fig. 6). Lys^{109} is the final water-mediated interaction between 3-OH and the protein. After Lys^{109}, only vdW interactions exist between the cholesterol and residues of the lid or binding tunnel opening in similar agreement with previous SMD simulations.14

In conclusion, based on the cv-SMD simulations, we propose a mechanism for sterol release from the bottom of the binding tunnel to the cytoplasm. This is conceptualized as two *molecular ladders* that guide the sterol from the bottom of the binding tunnel (Fig. 6). Several amino acids act as rungs in the *molecular ladders* during the exit of the sterol. Initially, two disjointed rungs Gln^{96}/Phe^{42} and Asn^{165}/Gln^{181} direct cholesterol release (Fig. 6, left). Phe^{42} forms a strong vdW contact with cholesterol (□4 to □8 kcal/mol). Then, water mediates interactions with two rungs, Gln^{96} and Gln^{181}, but these rungs are flexible and move up the ladder (down for uptake: Fig. 6, right). The final conceptualized rung is Lys^{109} that interacts weakly with 3-OH via water and vdW interactions with Ile^{206} and Pro^{211}. These two residues and those in the lid (Fig. 6) form strong vdW contacts with cholesterol at

the end of the SMD simulations. Previous SMD simulations14 suggested a process of cholesterol release to the cytoplasm that consists of (1) breaking water-mediated hydrogen bonds and vdW contacts, (2) opening of the lid cover, and (3) breakage of transient of sterol contacts with the rim. Our results agree with this work but focus mainly on the mechanism involved in the initial release of cholesterol (steps 1-2). In general, our *molecular ladder* mechanism is likely to exist with other sterols in *Osh*4 and the importance of the Lys^{109} rung will increase for hydroxylsterols because of its known interaction with this residue.6

Acknowledgments

This research was supported in part (J.B.K.) by the Intramural Research Program of the NIH (National Heart, Lung and Blood Institute). University of Maryland startup funds are also acknowledged (J.B.K.). The NIH Summer Internship Program (SIP) additionally supported this research through the National Heart, Lung, and Blood Institute at NIH (R.P.S.).

References

1. Yang HY. Nonvesicular sterol transport: two protein families and a sterol sensor? Trends In Cell Biology. 2006; 16(9):427–432. [PubMed: 16876994]
2. Lehto M, Olkkonen VM. The OSBP-related proteins: a novel protein family involved in vesicle transport, cellular lipid metabolism, and cell signalling. Biochimica Et Biophysica Acta-Molecular And Cell Biology Of Lipids. 2003; 1631(1):1–11.
3. Raychaudhuri S, Im YJ, Hurley JH, Prinz WA. Nonvesicular sterol movement from plasma membrane to ER requires oxysterol-binding protein-related proteins and phosphoinositides. J Cell Biol. 2006; 173(1):107–119. [PubMed: 16585271]
4. Prinz WA. Non-vesicular sterol transport in cells. Prog Lipid Res. 2007; 46(6):297–314. [PubMed: 17709145]
5. Beh CT, Rine J. A role for yeast oxysterol-binding protein homologs in endocytosis and in the maintenance of intracellular sterol-lipid distribution. J Cell Sci. 2004; 117(14):2983–2996. [PubMed: 15173322]
6. Im YJ, Raychaudhuri S, Prinz WA, Hurley JH. Structural mechanism for sterol sensing and transport by OSBP-related proteins. Nature. 2005; 437(7055):154–158. [PubMed: 16136145]
7. Schulz TA, Prinz WA. Sterol transport in yeast and the oxysterol binding protein homologue (OSH) family. Biochimica Et Biophysica Acta-Molecular and Cell Biology of Lipids. 2007; 1771(6):769–780.
8. Wang C, JeBailey L, Ridgway ND. Oxysterol-binding-protein (OSBP)-related protein 4 binds 25-hydroxycholesterol and interacts with vimentin intermediate filaments. Biochem J. 2002; 361:461–472. [PubMed: 11802775]
9. Klauda JB, Brooks BR. Sugar binding in lactose permease: Anomeric state of a disaccharide influences binding structure. J Mol Biol. 2007; 367(5):1523–1534. [PubMed: 17320103]
10. Isralewitz B, Baudry J, Gullingsrud J, Kosztin D, Schulten K. Steered molecular dynamics investigations of protein function. Journal of Molecular Graphics & Modelling. 2001; 19(1):13–25. [PubMed: 11381523]
11. Wang W, Donini O, Reyes CM, Kollman PA. Biomolecular simulations: Recent developments in force fields, simulations of enzyme catalysis, protein-ligand, protein-protein, and protein-nucleic acid noncovalent interactions. Annual Review of Biophysics and Biomolecular Structure. 2001; 30:211–243.
12. Murcia M, Faraldo-Gomez JD, Maxfield FR, Roux B. Modeling the structure of the StART domains of MLN64 and StAR proteins in complex with cholesterol. J Lipid Res. 2006; 47:2614–2630. [PubMed: 16990645]
13. Jensen MO, Yin Y, Tajkhorshid E, Schulten K. Sugar transport across lactose permease probed by steered molecular dynamics. Biophys J. 2007; 93(1):92–102. [PubMed: 17434947]
14. Canagarajah BJ, Hummer G, Prinz WA, Hurley JH. Dynamics of Cholesterol Exchange in the Oxysterol Binding Protein Family. J Mol Biol. 2008; 378(3):737–748. [PubMed: 18377932]

15. Brooks BR, Bruccoleri RE, Olafson BD, States DJ, Swaminathan S, Karplus M. CHARMM - a Program for Macromolecular Energy, Minimization, and Dynamics Calculations. J Comput Chem. 1983; 4(2):187–217.

16. Phillips JC, Braun R, Wang W, Gumbart J, Tajkhorshid E, Villa E, Chipot C, Skeel RD, Kale L, Schulten K. Scalable molecular dynamics with NAMD. J Comput Chem. 2005; 26(16):1781–1802. [PubMed: 16222654]

17. MacKerell AD Jr. Bashford D, Bellott M, Dunbrack RL, Evanseck JD, Field MJ, Fischer S, Gao J, Guo H, Ha S, Joseph-McCarthy D, Kuchnir L, Kuczera K, Lau FTK, Mattos C, Michnick S, Ngo T, Nguyen DT, Prodhom B, Reiher WE, Roux B, Schlenkrich M, Smith JC, Stote R, Straub J, Watanabe M, Wiorkiewicz-Kuczera J, Yin D, Karplus M. All-atom empirical potential for molecular modeling and dynamics studies of proteins. J Phys Chem B. 1998; 102(18):3586–3616.

18. Feig M, MacKerell AD Jr. Brooks CL. Force field influence on the observation of π-helical protein structures in molecular dynamics simulations. J Phys Chem B. 2003; 107(12):2831–2836.

19. MacKerell AD, Feig M, Brooks CL. Improved treatment of the protein backbone in empirical force fields. J Am Chem Soc. 2004; 126(3):698–699. [PubMed: 14733527]

20. Buck M, Bouguet-Bonnet S, Pastor RW, MacKerell AD. Importance of the CMAP correction to the CHARMM22 protein force field: Dynamics of hen lysozyme. Biophys J. 2006; 90(4):L36–L38. [PubMed: 16361340]

21. Pitman MC, Suits F, MacKerell AD, Feller SE. Molecular-level organization of saturated and polyunsaturated fatty acids in a phosphatidylcholine bilayer containing cholesterol. Biochemistry. 2004; 43(49):15318–15328. [PubMed: 15581344]

22. Durell SR, Brooks BR, Bennaim A. Solvent-Induced Forces between Two Hydrophilic Groups. J Phys Chem. 1994; 98(8):2198–2202.

23. Jorgensen WL, Chandrasekhar J, Madura JD, Impey RW, Klein ML. Comparison of Simple Potential Functions for Simulating Liquid Water. J Chem Phys. 1983; 79(2):926–935.

24. Darden T, York D, Pedersen L. Particle Mesh Ewald - an NLog(N) Method for Ewald Sums in Large Systems. J Chem Phys. 1993; 98(12):10089–10092.

25. Nosé S, Klein ML. A Study of Solid and Liquid Carbon Tetrafluoride Using the Constant Pressure Molecular-Dynamics Technique. J Chem Phys. 1983; 78(11):6928–6939.

26. Andersen HC. Molecular-Dynamics Simulations at Constant Pressure and/or Temperature. J Chem Phys. 1980; 72(4):2384–2393.

27. Hoover WG. Canonical Dynamics - Equilibrium Phase-Space Distributions. Phys Rev A. 1985; 31(3):1695–1697. [PubMed: 9895674]

28. Ryckaert JP, Ciccotti G, Berendsen HJC. Numerical Integration of the Cartesian Equations of Motion of a System with Contraints: Molecular Dynamics of n-alkanes. J Comput Phys. 1977; 23:327–341.

29. Isralewitz B, Gao M, Schulten K. Steered molecular dynamics and mechanical functions of proteins. Current Opinion in Structural Biology. 2001; 11(2):224–230. [PubMed: 11297932]

30. Izrailev S, Stepaniants S, Balsera M, Oono Y, Schulten K. Molecular dynamics study of unbinding of the avidin-biotin complex. Biophys J. 1997; 72(4):1568–1581. [PubMed: 9083662]

31. Humphrey W, Dalke A, Schulten K. VMD: Visual molecular dynamics. Journal of Molecular Graphics. 1996; 14(1):33–38. [PubMed: 8744570]

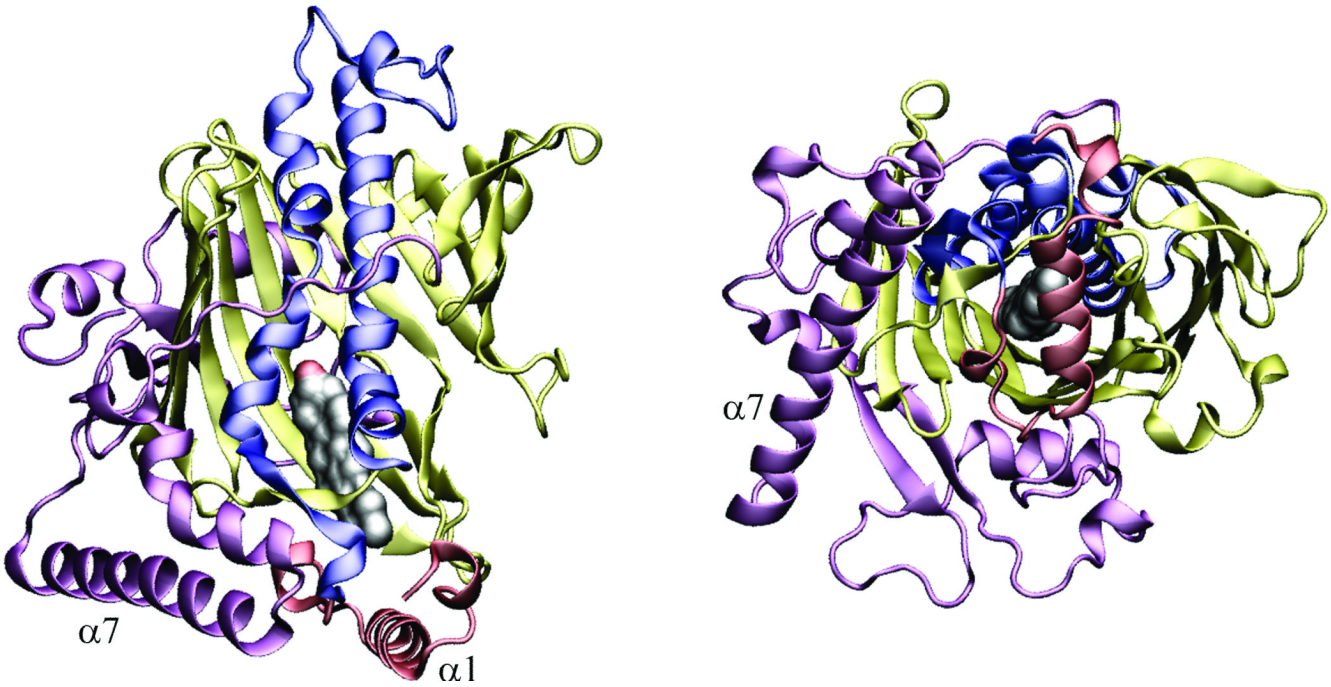

Figure 1.

The *Osh*4 crystal structure (1ZHY)6 and starting configuration for our simulations with cholesterol. Protein domains are color coded as follows: red □ protein lid, blue □ α-helix of ORD domain, yellow □ β-barrel of ORD domain, pink □ C-terminus. A side view (left) and view down the binding tunnel (right) are shown.

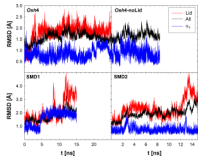

Figure 2.
The RMSD from the *Osh*4 crystal structure (1ZHY)6 of the backbone atoms for the entire protein, lid and α_7 helix for all simulations.

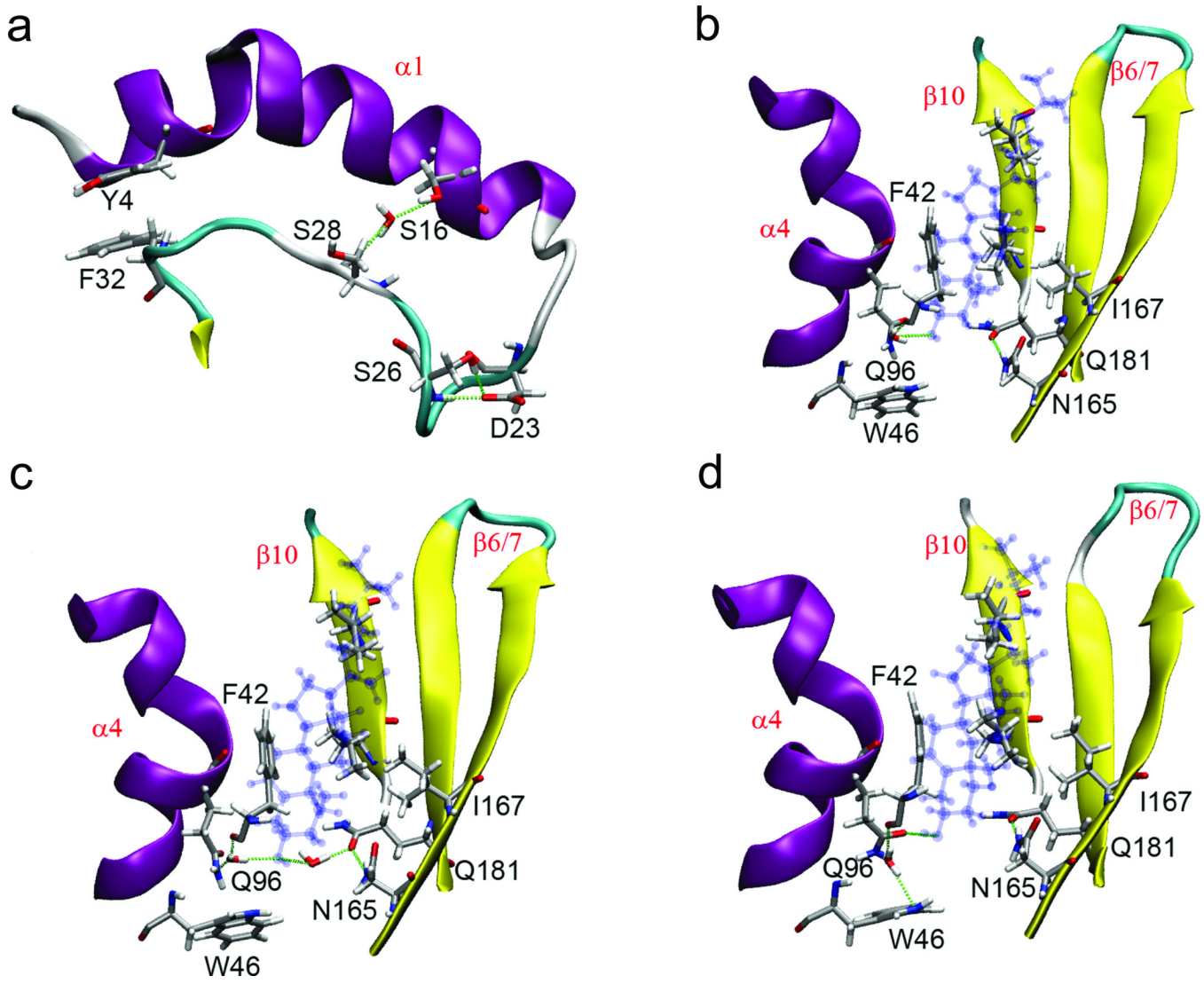

Figure 3.

The panel on the top left focuses on of the protein lid and interactions that stabilize it, whereas the last three panels focus on cholesterol/*Osh*4 binding. Snapshots are shown of cholesterol/*Osh*4/water configurations at (a) 24.75 ns, (b) 2.79 ns, (c) 6.37 ns, and (d) 24.97 ns. The important residues and secondary structure are labeled with black and red, respectively. Hydrogen bonds are labeled with dashed green lines and cholesterol in transparent blue. Two residues (Leu^{201} and Ile^{203}) on β_{10} are also shown because of their vdW interactions with cholesterol.

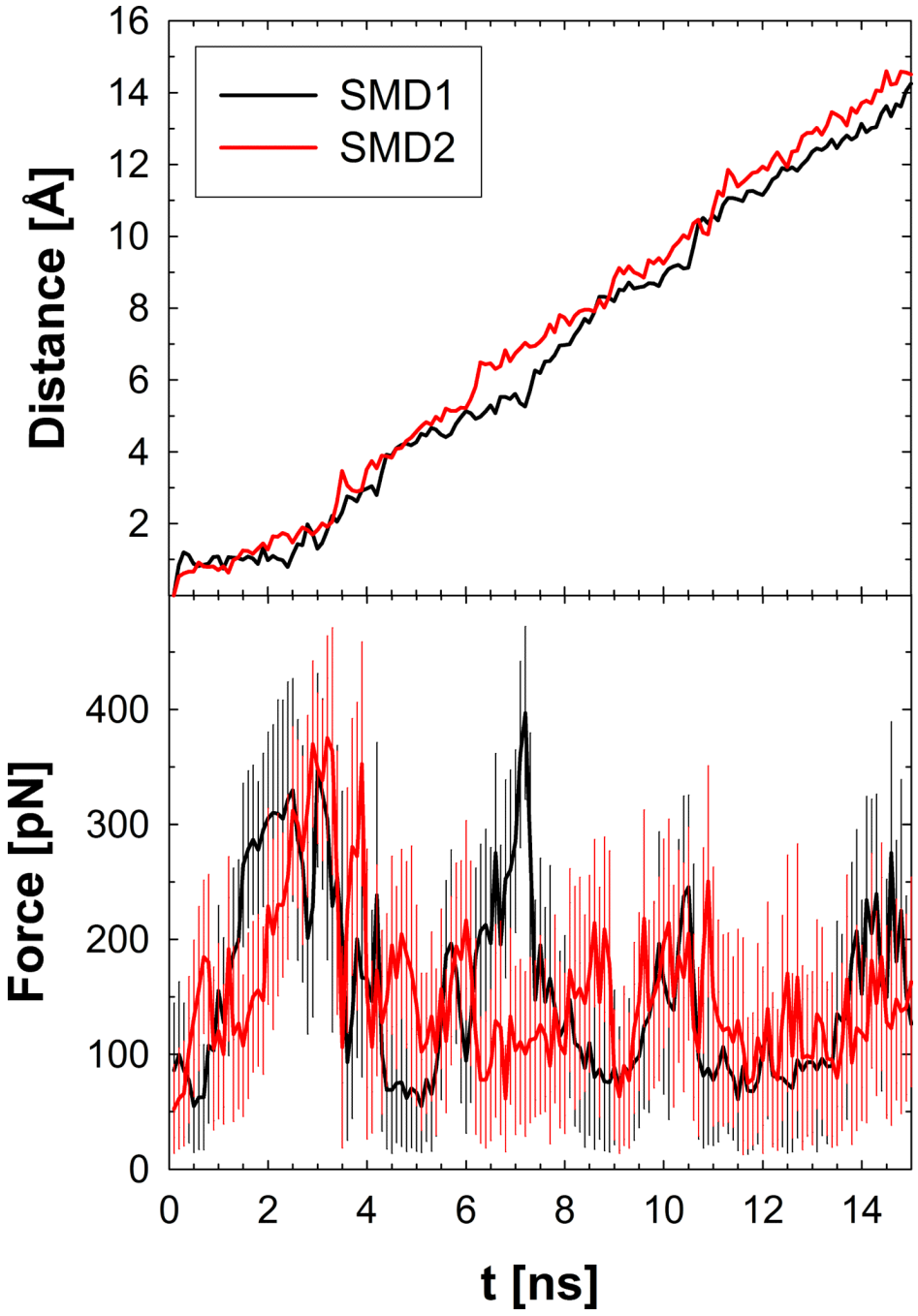

Figure 4.
The force (bottom) and distance (top) time series for the two cv-SMD simulations. For the SMD force, block averages (100 ps) are reported with their standard errors as vertical bars.

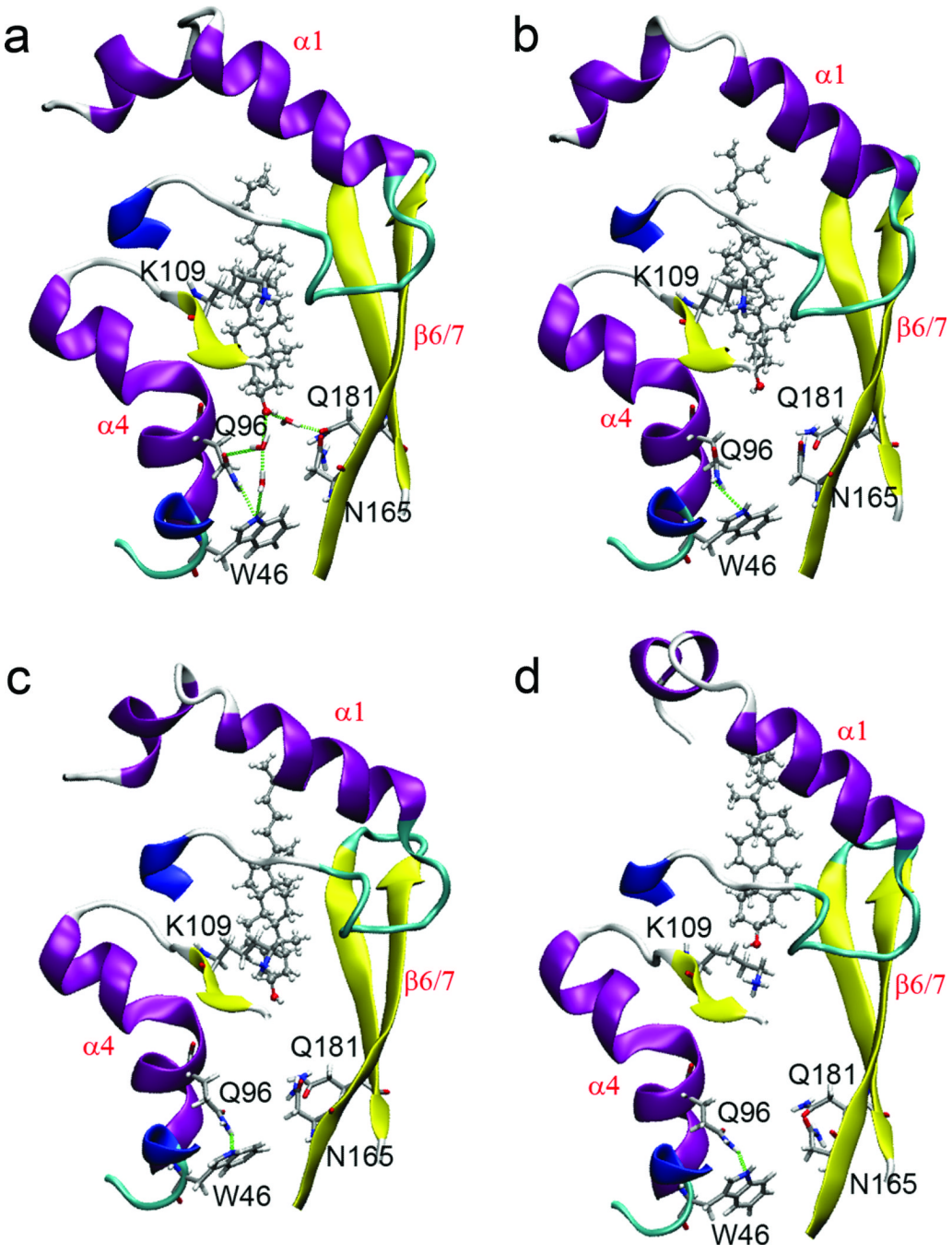

Figure 5.
Snapshots of cholesterol/protein/water configurations as it is pulled from the binding site (from a single run, SMD1): (a) 5.67 ns, (b) 7.35 ns, (c) 10.0 ns, and (d) 15 ns. The important residues and secondary structure are labeled with black and red, respectively. Hydrogen bonds are labeled with dashed green lines and vdW contacts are omitted for clarity.

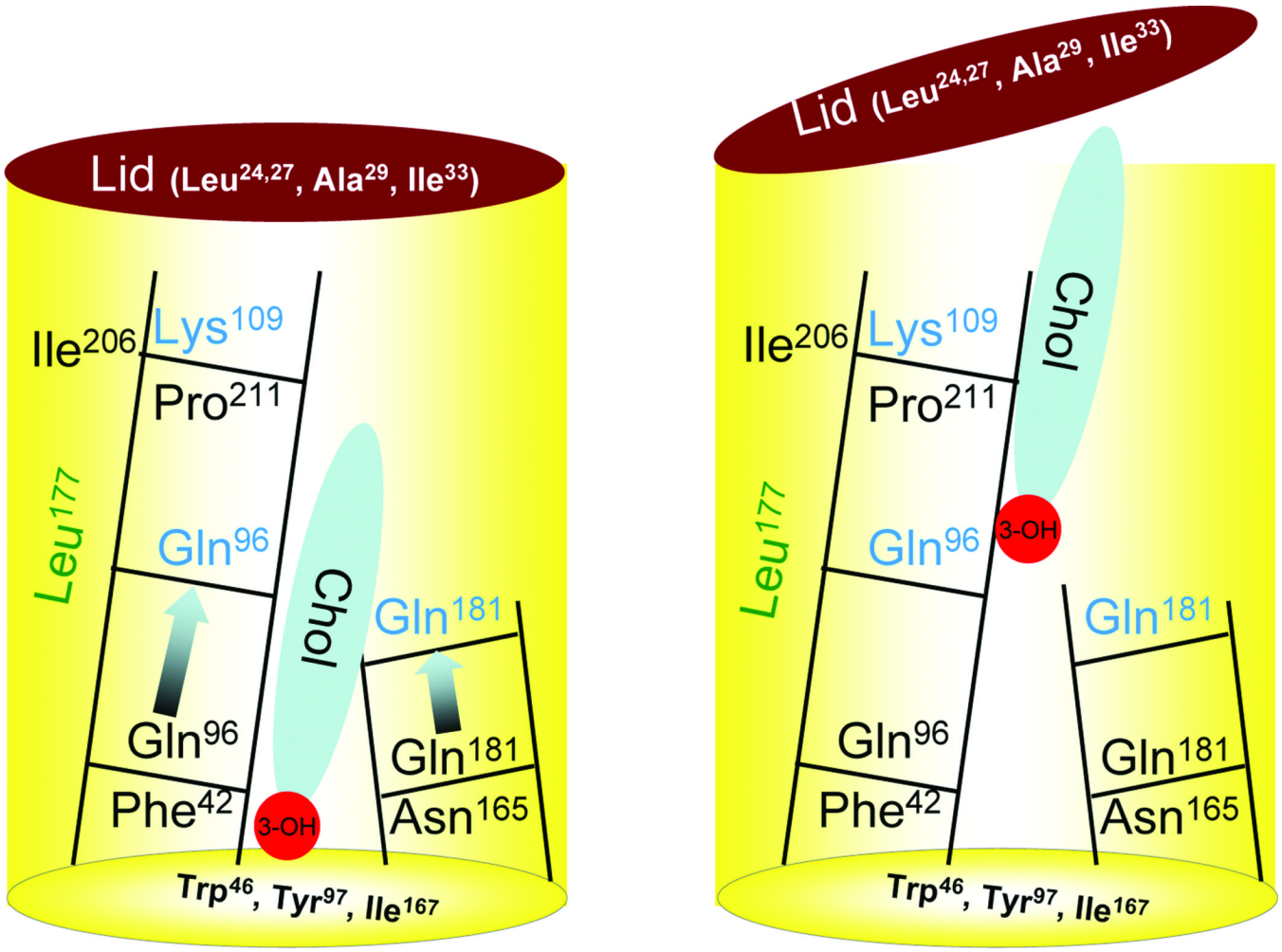

Figure 6.

A cartoon of the conceptualized *molecular ladder* of *Osh*4 to release/attract sterols to/from the cytoplasm and membrane. The β-barrel is visualized as a yellow cylinder, water-mediated interactions are colored in blue, and flexible/moving rungs are shown with arrows. The left cartoon is when cholesterol is in the binding pocket and interacts with the bottom rungs and two residues at the bottom of the barrel. The right cartoon is when cholesterol has moved up forming water-mediated interactions with and Gln^{96} and Gln^{181} and then begins to distort the lid. van der Waals contacts with certain residues of the lid are shown, as well as, Leu^{177} that interacts with cholesterol throughout its release. Transient interactions with the lid residues of Trp^{10}, Phe^{13}, Leu^{14}, Ile^{17}, and Phe^{20} are not shown but exist in the final stages of cholesterol release.

Table 1

Average interaction energies between protein residues and cholesterol. Only those that are approximately greater than 1.0 kcal/mol are listed. Thirteen non-polar residues are listed in the left with their vdW-only interaction energies and polar residues on the right (vdW+electrostatics)

Non-polar Residues	MD	MD-noLid	Polar Residues	MD	MD-noLid
Leu^{24}	□2.2±0.4	--	Trp^{46}	□1.1±0.5	□1.1±0.5
Leu^{27}	□0.7±0.2	--	Gln^{96}	□4.5±1.0	□4.4±0.9
Ile^{33}	□1.0±0.1	□1.2±0.2	Tyr^{97}	□3.9±0.3	□3.8±0.3
Leu^{39}	□2.0±0.2	□2.2±0.1	Asn^{165}	□2.1±0.5	□2.1±0.5
Phe^{42}	□4.1±0.3	□4.0±0.3	Gln^{181}	□1.5±0.5	□1.5±0.5
Ile^{167}	□2.4±0.1	□2.3±0.1	Lys^{109}	□2.7±0.2	□2.9±0.3
Leu^{177}	□1.1±0.2	□1.5±0.2			
Val^{179}	□1.0±0.2	□1.2±0.2			
Leu^{201}	□1.6±0.2	□1.6±0.2			
Ile^{203}	□2.6±0.2	□2.8±0.3			
Ile^{206}	□1.0±0.2	□1.3±0.2			
Pro^{211}	□0.9±0.1	□1.0±0.1			
Val^{213}	□1.1±0.1	□1.0±0.1			